



## Characteristics and fire-inducing risk analyses of arc faults in low-voltage electrical systems



Liwei Du<sup>a,b</sup>, Yulong Shen<sup>a,c</sup>, Zhihong Xu<sup>a,\*</sup>, Lijun Chen<sup>a</sup>, Duanyu Chen<sup>b</sup>

<sup>a</sup> College of Electrical Engineering and Automation, Fuzhou University, 350025, Fuzhou, China

<sup>b</sup> Department of Electrical Engineering, Yuan Ze University, 320315, Taoyuan, Taiwan

<sup>c</sup> Fujian Yongfu Power Engineering Co., Ltd., 300712, Fuzhou, China

### ARTICLE INFO

#### Keywords:

Arc fault  
Electrical fire  
Energy characteristics  
Ignition probability  
AFDD (arc fault detection device)

### ABSTRACT

Arc fault is a prevalent phenomenon in low-voltage residential power systems and the main cause of electrical fires. This paper explores the fire risks associated with arc faults and employs standards from arc fault detection devices (AFDD) to create an arc fault experimental system complemented by an integrated multi-sensor system for ignition related data collection. The objective is to synthetically examine the dynamic characteristics and ignition mechanisms of arc faults. This paper investigates the generation mechanisms, waveforms, and energy characteristics of arc faults, including waveform distinctions across different load types and patterns of energy variation during arcing. Data from the multi-sensor system become the cornerstone of the correlation analysis between the current, energy, and ignition phenomena, facilitating the construction of an ignition probability model based on maximum likelihood estimation. The reliability of the model is verified across various datasets with a 95 % confidence interval, offering a quantitative fire-inducing risk assessment of arc faults. Furthermore, the paper assesses the AFDD standards' break time limits and evaluates the performance of seven AFDD prototypes based on the proposed model, demonstrating the effectiveness of this technology in mitigating the risks of fires induced by arc faults. This study systematically analyzes the behaviors and ignition mechanisms of arc faults, thereby providing scientific evidence and data that support the enhancement of arc fault detection technologies and the development of fire prevention strategies.

### 1. Introduction

Arc fault is a prevalent residential electrical fault, involving electrical currents that travel through unintended paths in air or other media, potentially causing equipment damage or fires. These faults present serious challenges in prediction and detection due to randomness in both time and space. Despite these difficulties, studying arc faults is vital for the reliability of power systems and the safety of residential electricity usage. Researchers have extensively investigated arc faults, focusing on detection techniques, characteristic analysis, and simulation methods [1–4]. Various detection methods have been developed based on different principles to enhance the accuracy and response speed of arc fault identification [5,6,7]. Nonetheless, current knowledge about fires caused by arc faults remains predominantly qualitative. The specifics of how various intensities of arc faults ignite combustibles are not well-defined, underscoring the need for quantitative interpretation of the relationship between arc faults and fires to improve detection and

protection strategies.

The effects of arc faults on igniting combustibles due to damage to AC power lines are investigated through experimental observations of arc generation from both severed and intact conductors, as reported in [8], which provides crucial experimental evidence for assessing fire risks associated with damaged household appliance power cords. Detailed analyzes about the ignition characteristics of cotton as a fire indicator under varying current (2 A to 45 A) and time (10 s to 20 ms) conditions, according to the UL 1699 standard, are presented in [9], establishing a link between arc fault duration and ignition characteristics. In studies exploring the ignition capabilities of arc faults, reference [10] demonstrates that DC arcs significantly influence ignition time in materials used in photovoltaic systems, with absorbed power density and material thresholds being the critical factors. The study in [11] delves into the relationship between arc area and energy fluctuations, underlining the profound effects of arc current and combustion duration on fuel ignition likelihood. Additionally, the thermal characteristics of low-voltage AC

\* Corresponding author.

E-mail address: [fdxzh@fzu.edu.cn](mailto:fdxzh@fzu.edu.cn) (Z. Xu).

arc faults are explored in [12], finding that wire ignition time decreases as arc current increases. The specific causes of residential circuit fires initiated by arc faults are discussed in [13], which focuses on the chemical energy required to create a carbonized path at the site of cable damage and the energy necessary for series and parallel arc faults to initiate ignition. These conclusions further emphasize the direct relevance of arc fault energy to the occurrence of electrical fires.

Research into the energy characteristics during the arcing period of arc faults provides a crucial analytical dimension for assessing fire risks. In [14], a time-varying resistance model for AC arcs was developed to analyze the energy dynamics under various load conditions and establish a consistent relationship between arc fault energy and load characteristics. A method utilizing the concurrency rate of current spikes and a specific energy assessment was applied in [15] to gauge the severity of parallel arc faults in DC aviation power systems. While these researches studied the energy characteristics of arc faults in detail, they did not explore the quantitative relationship between variations in fault energy and specific ignition phenomena.

Arc fault circuit interrupters (AFCI) or arc fault detection devices (AFDD) are designed to mitigate line erosion from arc faults and reduce the likelihood of fire incidents, as noted in [16,17]. Despite their utility, AFCI/AFDD devices exhibit a certain delay in interrupting faults, revealing a gap in protective effectiveness against arc fault induced ignition risks. The effectiveness of AFDD in maintaining the energy of series arc faults below a 100 J threshold was examined in [18]. This investigation highlighted that standards relying on time estimation rather than direct measurement of arc energy do not effectively constrain the energy levels of arcs. Unfortunately, the paper did not include test results or analysis for scenarios where energy exceeded the threshold and led to ignition.

Reference [19] suggests that the energy required to sustain an arc flame remains relatively constant under specified conditions, encompassing both carbonization and ignition stages. However, without distinguishing their individual energy contributions, the generalizability of the findings is limited. Experiments on series arc faults in 220 V HIV cables indicate that the total energy released by arc faults maintains a consistent level during the ignition process for varying load currents [20]. This consistency is corroborated by the findings in [21], which posit that a fixed amount of energy is necessary to ignite a given quantity of material, assuming that the ignition phase is brief enough to prevent excessive energy loss through conduction or convection so that the arcs remain stable. Reference [22] explores how series arcs ignite silicone rubber sheaths under different supply currents and arc durations, establishing a functional relationship between ignition probability and arc energy, thus providing a novel approach to evaluating fire risks associated with arc faults. However, most current research focuses on specific experimental conditions, resulting in a lack of comprehensive understanding of arc fault ignition phenomena across diverse conditions. Moreover, the stability and consistency of arcing states significantly influence both the ignition time and the likelihood of fire incidents [23].

Despite the extensive foundational research on understanding and detecting arc faults, studies of ignition characteristics under various conditions remain insufficient. Consequently, this paper develops an experimental system for arc faults, based on the IEC 62606 and GB 14287 standards, to systematically investigate the dynamic characteristics of arc faults and corresponding ignition probability, aiming to enhance the understanding of arc fault induced fire incidents and prevention. The contributions of this paper include:

- 1) The introduction of a new method for collecting diverse data types related to arc fault induced ignition, particularly under dynamically changing conditions.
- 2) In-depth analyzes of arcing processes across various conditions reveal distinct arc-fault patterns in energy distribution and waveform changes.

- 3) The development of a probability model for ignition based on the experimental data offers new insights into the understanding and prevention of arc fault induced fires.
- 4) Experimental analysis of the limit breaking time as defined by standards and seven AFDDs, quantifies the ignition risk caused by arc faults under protected conditions.

This paper is organized into six sections. Following the introduction, Section 2 describes the arc fault experimental system and the arc generation process. Section 3 examines the waveforms and energy characteristics of arc faults. In Section 4, comprehensive ignition data are collected to discuss the relationship between arc fault current/energy and ignition probability, for the development and evaluation of the ignition probability model. Section 5 performs a quantitative analysis of the AFDD standards and products. Finally, Section 6 summarizes the paper and proposes future research directions.

## 2. Experimental system and arcing phenomenon

Arc faults display randomness in time and space under various conditions during the arcing period, complicating the data capture in practice. To guarantee the authenticity of the collected data, this paper constructs an arc fault experimental system according to the dynamic characteristic study requirements in IEC 62606 [24] (akin to GB/T 31143 [25]) and GB 14287.4 [26].

### 2.1. Configuration of the arc fault experimental system

Due to the diverse testing requirements specified by standards, arc fault experimental systems that comply with these criteria are often complex to operate. Consequently, this paper constructs an integrated system for arc fault experiments according to standardized experimental protocols, shown in Fig. 1. The system comprises four main components: (a) arc fault generation devices, (b) the main experimental circuit, (c) data collection and circuit switching control/feedback modules, and (d) a supervisory computer operating platform.

Arc faults are simulated using three types of arc generation devices, as required by standards IEC 62606, GB/T 31143, and UL 1699 [27], shown in Fig. 1-(a). Each device is designed to replicate one of specific real-world fault scenarios.

- The arc generator with movable and fixed electrodes that separate from each other to a distance during energization to generate arc faults, realistically simulates faults caused by loose contacts, poor terminal connections, or conductor breaks.
- The carbonized cable device applies varying high voltages to a taped cable at an incision of the cable, creating a carbonized conductive path. This prepared carbonized cable specimen accurately replicates arc faults resulting from insulation damage, aging, carbonization, or high-temperature deterioration, closely resembling real-world insulation failures.
- The guillotine adopts a metal knife switch to sever two closely spaced cable circuits at the same time during energization, realistically simulating interphase metallic short-circuit arc faults resulting from external metal impacts, cutting, or cable crushing in actual electrical systems.

These diverse arc generation methods enable the experimental system to produce a broad range of fault types that closely resemble arc faults occurring in residential and commercial electrical systems, thereby ensuring the realism and comprehensiveness of the simulations.

Fig. 1-(b) illustrates the main circuit topology of the experimental system and the logical relationships among the components, designed to simulate low-voltage residential electrical networks. The circuit comprises a power supply (coupling transformer), long/short-distance lines, arc fault generation devices, and various loads.

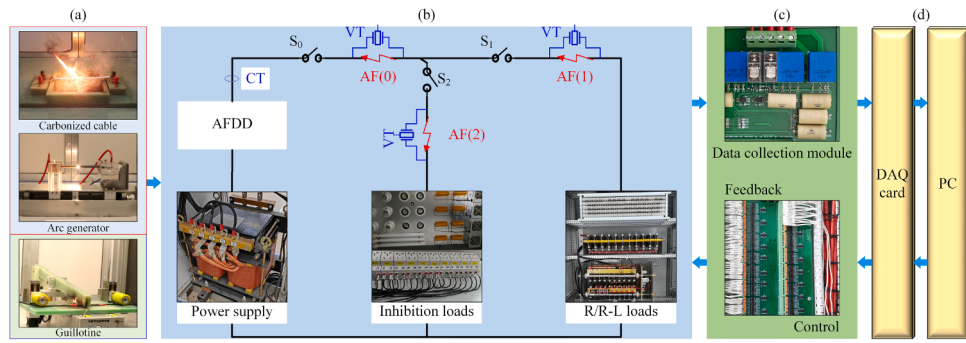


**Fig. 1.** Integrated arc fault experimental system.

Arc fault settings at AF(0), AF(1), and AF(2) induce faults at various locations and times, simulating different fault scenarios. Switches S(0), S(1), and S(2) enable dynamic circuit reconfiguration, facilitating the replication of diverse network topologies. Multiple current and voltage sensors monitor line currents and arc voltages. The load configurations include R/R-L, inhibition, and interference loads, mimicking typical residential and commercial electrical loads and combinations of above-mentioned loads. This comprehensive setup allows for the control of fault injection and circuit switching, enabling the recreation of a broad spectrum of load conditions and topologies. The configurations cover simulations specified in Section 9.9 of GB/T31143 and IEC 62606, encompassing most scenarios likely encountered in residential electrical networks.

It is crucial to note that the arc fault current in this setup represents the prospective current in the circuit prior to the arcing period, considering the total impedance of the circuit, including the source equivalent impedance. This distinction helps to more accurately represent the characteristics of residential circuits, as opposed to distribution network systems.

Figs. 1-(c) and (d) illustrate the interaction between the supervisory computer and the subordinate machine within the experimental system. The data acquisition (DAQ) card transmits the collected current and voltage data, along with feedback from the control board in the experimental circuit and arc generation device, to the supervisory computer. This process enables the supervisory computer to control the switches of the experimental circuit via the relay control board. The supervisory computer precisely manages the arc fault generation process by coordinating the timing and sequencing of events via DAQ cards.

This experimental system facilitates automated switching between devices to appropriate nodes in the circuit, tailored to meet various experimental requirements through the coordinated control of components. Featuring diverse arc generation methods, precise control mechanisms, and advanced data acquisition systems, it enables the simulation of a broad spectrum of arc faults under controlled conditions. By precisely manipulating parameters such as electrode gap width, carbonization level, and cutting speed, the system accurately generates arc faults that closely resemble the ones occurring in real-world residential and commercial electrical systems. This comprehensive approach provides realistic conditions for studying the dynamic characteristics of arc faults, significantly enhancing the validity and applicability of the research findings in this field.

## 2.2. Observations of diverse arcing mechanisms

The mechanisms of arc formation vary significantly based on the discharge media utilized in various generation methods. Specifically, arcs in carbonized cable experiments are predominantly caused by the conductivity of carbon residue (graphite particles) within the carbonization path under electrified conditions, with the carbon residue acting as the primary discharge medium. In these experiments, the space between two conductors in pre-carbonized cables is filled with carbon

powder. The dynamics and intensity of arc combustion are influenced by the carbon residue's distribution density within the cable incision [28], resulting in relatively stable and continuous arcs as the carbon provides a consistent conductive path. Conversely, arcs can also be generated by arc generators with the ionization of air between two separated electrodes upon electrification, with air serving as the main discharge medium. In this setup, a specific gap between the electrodes is maintained to produce arcs. Factors such as electrode material, separation speed, and electrode distance significantly affect the dynamics of arc combustion, typically characterized by high temperatures and bright light [29]. The ionization process in air-mediated arcs leads to more dynamic and potentially unstable arcs, influenced heavily by environmental factors and electrode conditions.

Discharge media profoundly influence arc characteristics. Carbon residue-mediated arcs are more localized within the conductive path and typically exhibit lower temperatures under normal conditions compared to the air-mediated ones, as the energy is more evenly distributed through the carbon particles. However, when the carbonization path is confined by insulating materials such as PVC and fiberglass tapes, localized heating can build up pressure and result in more explosive, jet-like flames. Air-mediated arcs can reach higher temperatures and exhibit explosive behaviors due to rapid air ionization and expansion, particularly in open environments. Additionally, carbon residue-mediated arcs are easier to initiate due to the pre-existing conductive path, whereas air-mediated arcs require a higher breakdown voltage to ionize the air gap. The conductivity of carbon residue remains relatively constant during arcing, although it may increase slightly with temperature in confined spaces, whereas the conductivity of air changes dramatically upon ionization. Variations in experimental conditions (voltage, current), environmental factors (temperature, humidity), and specific experimental details (cable, electrode parameters) are also influential factors for the differing physical and electrical characteristics of arcs generated by various methods.

Paschen's law indicates that the breakdown voltage changes with gas pressure and gap width between electrodes. Under the specific condition of narrow gaps, the breakdown voltage of air under standard atmospheric pressure is typically higher than residential grid voltage, making it difficult to form a continuous arc between two copper electrodes. However, graphite electrode, which has higher electron emissivity and a lower work function, can facilitate electron emission and sustain continuous arcs at reduced voltages [30]. Therefore, an arc generator using one graphite electrode paired with one copper electrode can significantly reduce the voltage threshold for the generation of continuous arcs. A graphite electrode, paired with a copper electrode in the arc generator, facilitates thermal ionizing current generation. Initially, the electrodes are in contact, allowing normal current flow, as shown in Fig. 2-(a). A stepper motor controls the movable electrode, retreating from the fixed electrode. Upon reaching a specific separation, a stable arc forms, as shown in Figs. 2-(b) and (c). During the early phase of separation, the jetting arc plasma may short-circuit the electrodes without a noticeable arc phenomenon for minor gaps (10 μm). For the

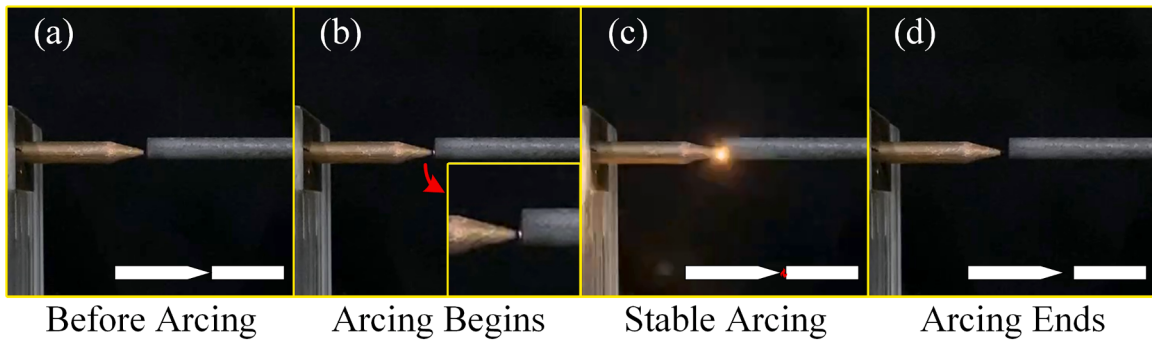


Fig. 2. Arcing process using arc generator.

given electrode materials, the arc voltage remains nearly constant within a certain range, and the arc's maintenance primarily relies on the current. After the experiment, the electrodes continue to separate until the arc can no longer be reignited, signaling an open circuit, as shown in Fig. 2-(d).

The cable specimens for the carbonized path experiment prepared through high-voltage electrification are shown in Fig. 3-(a). When connected to the experimental circuit and energized, the arc forms in the carbonized path at the incision. During electrification, the arc intensity affects the dynamic stability of the carbonized path. This arc may either maintain the carbonized path by decomposing or igniting the uncut cable insulation around the cable incision, as shown in Fig. 3-(b); alternatively, it may eject carbon residue at the incision due to excessive current energy, resulting in the rupture of the carbonized path or the fusion of the conductors, as shown in Fig. 3-(c). Post-experiment, small holes formed by arcing or ejection are visible near the tape-wrapped incision, as shown in Fig. 3-(d).

Interphase or ground parallel arc fault currents are relatively higher under normal conditions, and conventional protection devices typically provide adequate protection against such faults. Related devices and experiments are not further discussed since this paper focuses primarily on series arc faults in low-voltage conditions.

To ensure reproducibility and facilitate fair comparison, all parameters for the carbonized cable specimens and arc generators discussed in this paper are set according to the specifications in IEC 62606. Control strategies for the arc generator and the preparation of carbonized cables follow methodologies described in previous studies [28,31]. It is crucial to note that the cable material can significantly influence arc behavior. This study focuses mainly on low-voltage residential cable, which predominantly adopts PVC insulation, specifically "PVC insulation + copper conductor" cables. Following international standards such as IEC 62606, UL 1699, and GB/T 31143, PVC-insulated cables are used to prepare carbonized cable specimens for simulating arc faults.

The experiments involved cables from various manufacturers, including Panda, Delixi, and Far East Cables, covered different cable

types such as RVVB, BVVB, and BVR. This varied selection ensures a comprehensive representation of commonly used residential cables, accounting for variations in PVC insulation parameters. As demonstrated in [28], precise control methods are employed to ensure that cable specimens prepared from various cables comply with relevant standards. This methodology maintains consistency in the experiments while accommodating potential variations due to different cable materials.

### 3. Waveform and energy dynamics of arc faults

Voltage and current data for various types of arc faults are obtained using the arc fault experimental system. This section conducts a comprehensive analysis of the key characteristics of arc fault waveforms, examining the typical features of resistive arc faults and delineating waveform differences across various conditions. Additionally, an analysis of energy performance during the arcing process under different conditions is provided, offering a unique perspective for understanding arc faults.

#### 3.1. Waveform characteristics of typical arc faults

Both voltage and current waveforms exhibit significant distortion when an arc fault occurs. The arc voltage waveform appears saddle-shaped, displaying arcing and extinguishing peaks within each half-period, as shown in Fig. 4. The arc current waveform shows a 'shouldering' phenomenon at the zero crossing, characterized by a higher rise rate post-zero crossing than normal current and a slight decrease in amplitude.

During the arcing phase, the arc current  $I_{arc}(t)$  begins to rise from zero while the equivalent arc resistance  $R_{arc}(t)$  decreases after reaching the arcing peak ( $U_{ap}$ ). Subsequently, the arc voltage  $U_{arc}(t)$  falls below the supply voltage  $U(t)$  and diminishes further as  $I_{arc}(t)$  increases, eventually stabilizing at a relatively steady value. As  $I_{arc}(t)$  gradually diminishes from its peak,  $U_{arc}(t)$  rises to the extinguishing peak ( $U_{ep}$ ),

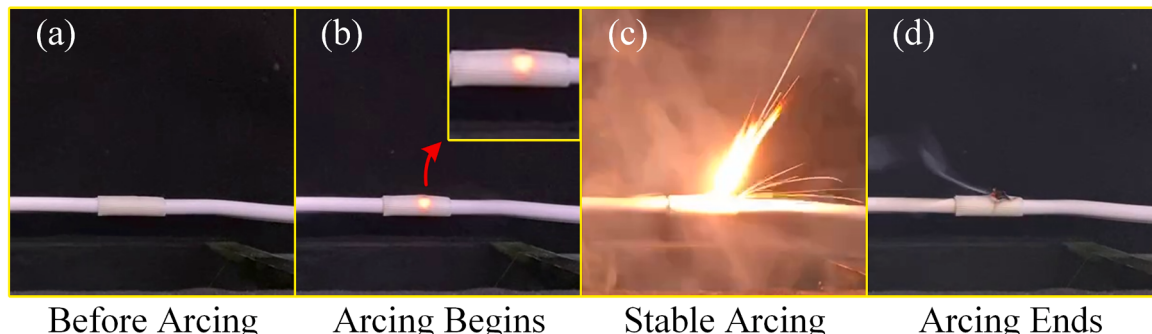


Fig. 3. Arcing process using carbonized cable specimen.

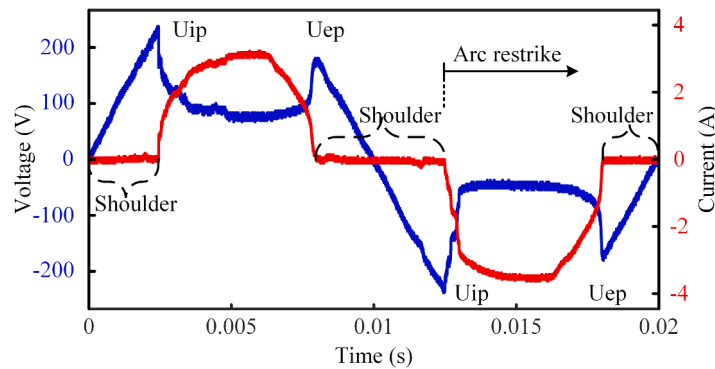


Fig. 4. Typical arc fault voltage/current signals.

and  $R_{arc}(t)$  increases. Throughout the arcing half-period,  $U_{ep}$  remains less than  $U_{ap}$ . The rise rate of  $R_{arc}(t)$  is slower due to the thermal inertia of the arc column, and it lags behind when  $I_{arc}(t)$  increases.  $I_{arc}(t)$  is governed by the ratio of  $U(t)$  to the total line impedance ( $Z$ ) (i.e.,  $R_{arc}(t) + R_2$ ), where  $I_{arc}(t) = U(t)/Z$ .  $R_{arc}(t)$  during the arcing phase is relatively low, resulting in  $I_{arc}(t)$  being slightly lower than the rated current. During the extinguishing phase, as arc power wanes, the arc cannot sustain continuous combustion.  $U_{arc}(t)$  aligns with  $U(t)$  during the waveform phase from  $U_{ep}$  to the reverse  $U_{ap}$ . In this phase,  $R_{arc}(t)$  tends toward infinity, and  $I_{arc}(t)$  approaches zero, leading to the so-called shoulder phenomenon. The shoulder persists until the arc is reignited in the reverse half-period.

These waveform changes are typically periodic. With sufficient power, the arc can extinguish and be reignited periodically in synchronization with the inherent frequency of the AC power source. Furthermore, the oscillatory characteristics of  $R_{arc}(t)$  introduce high-frequency components into the arc waveform, further complicating the electrical characterization of arc faults.

### 3.2. Comparative analysis of arc fault waveforms

During the operation of the arc generator, the waveform characteristics of the arcing process, resulting from the separation of graphite-copper electrodes under electrification, are complex, with neither voltage nor current exhibiting apparent periodicity. As shown in Fig. 5-(a), in the initial stage of electrode separation,  $R_{arc}(t)$  is minimal, the arc voltage amplitude remains relatively low, resembling a rectangular shape without distinct  $U_{ap}$  and  $U_{ep}$  peaks, and the shoulder phenomenon in the arc current is subdued. The arc voltage and current exhibit stable characteristics similar to typical arc faults upon reaching a stable arc distance. Additionally, the control strategy of the electrodes influences the arc waveform produced by the arc generator, resulting in a voltage waveform with gradually increasing amplitude as the moving electrode separates progressively, as detailed in [32].

In cable specimens where a carbonized path has successfully formed,

the carbon residue content at the incision ensures arc stability for a brief period. As shown in Fig. 5-(b), post-electrification, the arc sustains continuous and stable combustion, with voltage and current waveforms mirroring the periodic characteristics of the original power source. The arc voltage waveform presents a typical saddle shape, displaying periodic symmetry between  $U_{ap}$  and  $U_{ep}$ . The shoulder phenomenon in the arc current is more pronounced and maintains a stable duration.

Section 9.9.4.2 of the standards IEC 62606 and GB/T 31143 enumerates common types of operation inhibition loads found in residential environments, including vacuum cleaners, electronic switching mode power supplies, capacitor start motors (air compressor type), electronic lamp dimmers, fluorescent lamps, halogen lamps powered by electronic transformers, and electric hand tools [33]. These loads may display characteristics similar to those of arc fault currents during their operation, particularly leading to more complex waveforms when arc faults occur. Experiments involving various load types are performed following the experimental methods outlined in section 9.9.2.2 of the IEC 62606 standard, utilizing the circuit connection detailed in Figure A11, Configuration A [24,25]. Arc faults are initiated near the 0.1 s mark using a carbonized path specimen.

Vacuum cleaners, capacitor start motors, and electric hand tools exhibit inrush phenomena at startup, which subsequently stabilize at a lower operational current level. These loads have distinct periodic characteristics in their current waveforms when operating stably but differ from one another. Unlike the typical sinusoidal waveforms of general linear loads, most residential loads usually exhibit non-sinusoidal waveforms during stable operation, as shown in Fig. 6. The currents of electronic switching mode power supplies and tungsten loads with an electronic lamp dimmer maintain a continuous and stable shoulder. Due to the electronic ballasts in fluorescent lamps and electronic transformers in halogen lamps, their waveforms are approximately sinusoidal with high-frequency components. The waveform of electric hand tools typically appears as a triangular wave, whereas vacuum cleaners and capacitor start motors display nearly triangular waves with shorter shoulders.

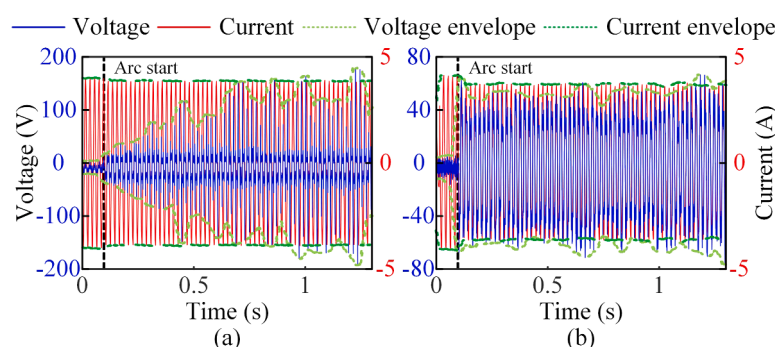
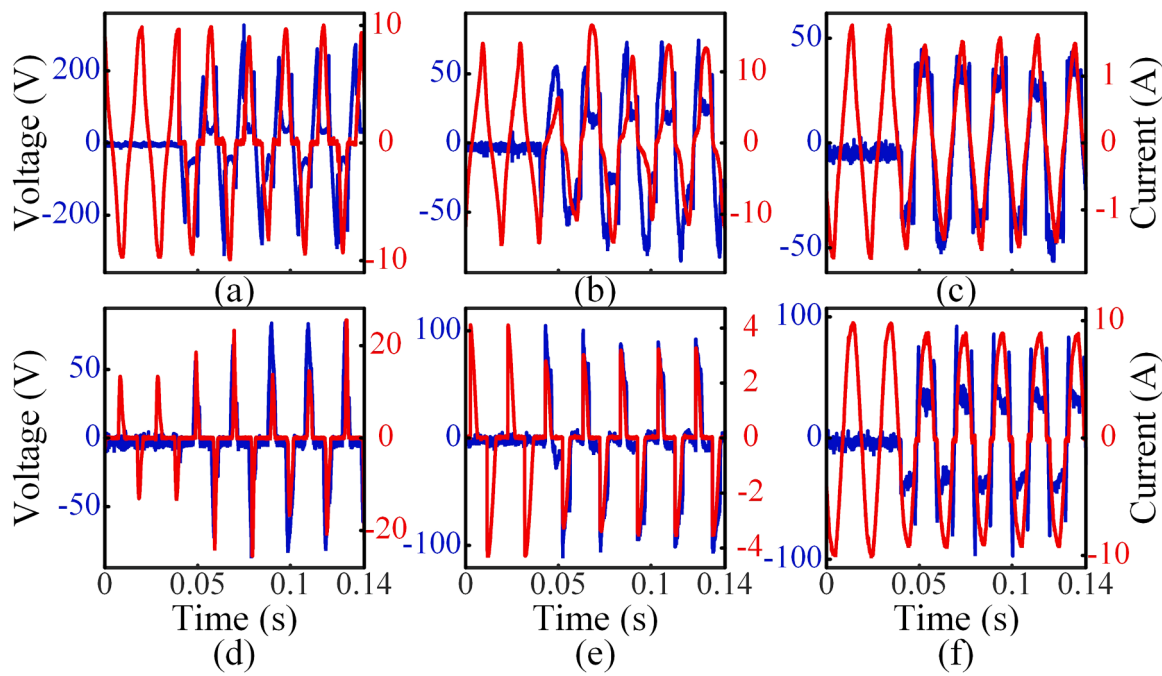


Fig. 5. Fault signals at 3A for different arc generation devices. (a) Arc generator, (b) Carbonized cable.



**Fig. 6.** Voltage/current signals under different inhibition loads. (a) vacuum cleaner, (b) capacitor start motor, (c) electric hand tool, (d) electronic switching mode power supply, (e) electronic lamp dimmer, (f) halogen lamps.

When various loads experience arc faults, their waveform characteristics undergo abnormal changes. The high-temperature channel created by the arc fault directs the current along unintended paths, leading to atypical high-amplitude spikes and irregular fluctuations in the originally stable current waveform. The voltage waveform may also experience transient decrease or instability, as depicted in Fig. 6. Specifically, loads with motors may show more pronounced current fluctuations due to the influence of internal inductance. Loads governed by power electronic control mechanisms display irregular current and voltage waveforms due to discrepancies between the arc faults-induced circuit break/closure and the control circuit, often manifesting as half-wave losses. Additionally, arc faults disrupt the precise control of lamp load controllers, leading to abnormal spikes and fluctuations in the current waveform. These diverse and random changes result from the nonlinear conductive characteristics of the arc and its impact on system impedance. Furthermore, the duration of an arc fault may be prolonged under these inhibition loads.

### 3.3. Energy dynamics of arc faults

In the process of arc faults leading to fires, various forms of energy manifest uniquely and interact via specific physical and chemical mechanisms, ultimately causing the combustion of cable insulation or external combustibles. The total energy of an arc fault ( $Q_{\text{arc}}$ ) can be expressed as:

$$Q_{\text{arc}} = Q_{\text{main}} + Q_{\text{radiation}} + Q_{\text{splashing}} + Q_{\text{chemical}} + Q_{\text{other}} \quad (1)$$

where  $Q_{\text{main}}$  is the energy directly released during the arc discharge process and constitutes the primary fire risk;  $Q_{\text{radiation}}$  represents the energy from light and thermal radiation emitted by the arc;  $Q_{\text{splashing}}$  pertains to the energy from molten metal splashes due to high temperatures;  $Q_{\text{chemical}}$  is the energy released through chemical reactions; and  $Q_{\text{other}}$  includes energy in various other forms.

$Q_{\text{main}}$  and  $Q_{\text{radiation}}$  are critical for ignition resulting from arc faults, as they directly contribute to the heating and combustion of materials. During cable combustion, the arc directly heats the cable, bringing the insulation material to its ignition point and initiating combustion.

Chemical reactions within the cable material may accelerate this process. Additionally, even if external combustibles are some distance from the arc source,  $Q_{\text{radiation}}$  and  $Q_{\text{splashing}}$  can still directly impact the surrounding combustibles, with  $Q_{\text{radiation}}$  heating object surfaces and molten metal particles providing a direct heat source. The arc fault experimental system described in Section II enables the convenient acquisition of voltage and current signals, allowing for the real-time calculation of  $Q_{\text{arc}}$  as:

$$Q_{\text{arc}} = \int_0^t P_{\text{arc}}(t) dt = \int_0^t U_{\text{arc}}(t) \cdot I_{\text{arc}}(t) \cdot H(|I_{\text{arc}}(t)| - 0.05I_e) dt \quad (2)$$

$$\text{s.t. } H(x) = \begin{cases} 0 & \text{if } x \leq 0 \\ 1 & \text{if } x > 0 \end{cases}$$

where  $P_{\text{arc}}(t)$  represents the instantaneous power of the arc fault at time  $t$ ;  $H(x)$  functions to eliminate currents that do not exceed 5 % of  $I_e$  amplitude before and after each current flow;  $I_e$  denotes the expected current level.

The energy released by an arc fault is determined by the current and voltage, where the  $I_e$  in the circuit significantly influences  $Q_{\text{arc}}$ . Due to the shoulder effect of the arc fault current, the energy curve exhibits a stepped pattern with gentle fluctuations. An increase in current typically results in an accelerated energy release because the high current and corresponding voltage together produce greater power output. This leads to an increase in the slope  $k$  of the linear fit curve for energy accumulation, as shown in Fig. 7. This indicates that as the current increases, so does the energy released per unit. Additionally, it is observed that arc faults generated by carbonized cable specimens demonstrate relatively stable energy variations within the utility frequency period range.

Further observations reveal that the experimental results from the arc generator align with the IEC standard's breaking characteristics, enhanced by a factor of 2.5. The assumption by the IEC that the arc power of short series arcs produced by an arc generator is 2.5 times lower than those generated by cable experiments is validated [18].

Arc faults are inherently hazardous and can lead to residential fires, with their danger influenced by factors including the intensity and duration of the arc fault. High-current arc faults, such as those at 40A,

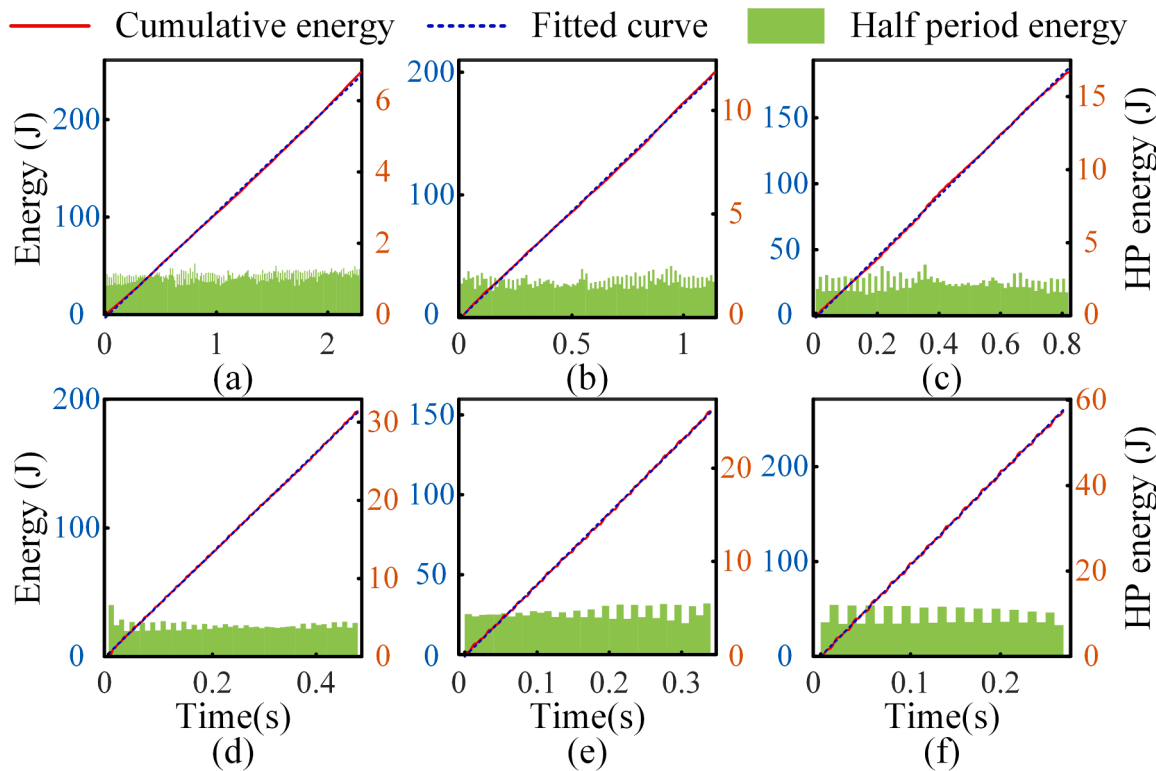


**Fig. 7.** Arc fault energy and its fitting curves for different current settings. (a) 3A,  $k = 108.13$ , (b) 6A,  $k = 175.88$ , (c) 10A,  $k = 223.07$ , (d) 16A,  $k = 416.17$ , (e) 20A,  $k = 451.95$ , (f) 40A,  $k = 960.42$ .

pose a greater fire risk because they can release a lot of energy in a short time, although often lasting only a few periods. Conversely, a lower-current fault like 5A, though slower in energy release, can persist for longer durations. Thus, all arc faults, irrespective of current magnitudes, must be treated with caution as they all possess the potential to ignite fires under certain conditions.

The energy accumulation in an arc fault is critical for understanding and predicting the associated fire risk, arc fault energy is strongly correlated with the danger of ignition. Rapid accumulation and release of arc fault energy can significantly shorten the necessary time for igniting external combustibles, thereby increasing the likelihood of a fire. Therefore, the energy produced by an arc fault and its potential to cause ignition under different conditions must be carefully considered.

#### 4. Correlation between arc fault energy and ignition of external combustibles

The accumulation of energy during the arcing period directly influences the timing and likelihood of arc faults igniting external combustibles. This characteristic serves as a critical parameter for assessing the fire risk associated with arc faults. To gather pertinent data on ignition, a multi-sensor collection system designed to ignite external combustibles by arc faults is developed, utilizing a carbonized cable device. A probability model based on maximum likelihood estimation (MLE) is proposed to address the variability of ignition data in arc faults. This model facilitates the analysis of ignition probabilities under various conditions.

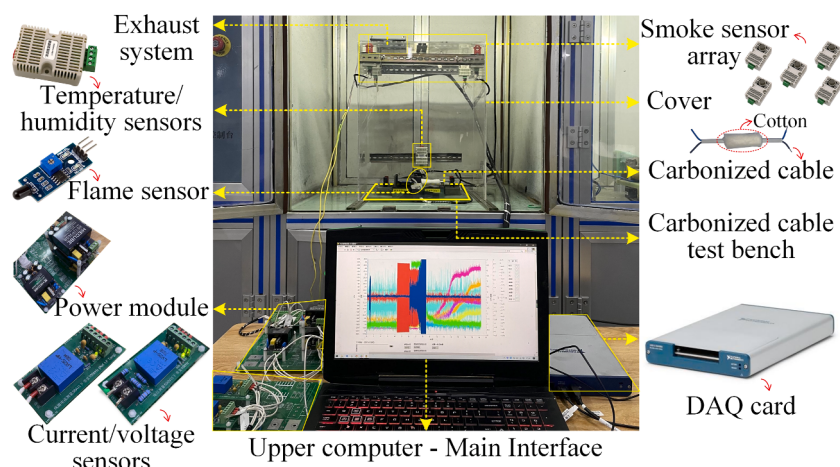


**Fig. 8.** Integrated multi-sensor data acquisition system.

#### 4.1. Integrated multi-sensor data acquisition system

An arc fault ignition data collection system equipped with multiple sensors is developed using the carbonized cable device described in Section II to study the relevance between arc fault energy and ignition behavior, as shown in Fig. 8. The carbonized cable device is enclosed within a transparent cover, which can be sealed or ventilated to simulate different environmental conditions for arc faults. Following the UL 1699 standard [27], 100 % pure cotton, a common highly flammable material in residential environments, is utilized as a combustion indicator to demonstrate the ignition capabilities of arc faults with minimal energy. Uniform layers of cotton are wrapped around the incision of the carbonized cable specimen, where the arc fault is generated.

To precisely monitor the physical parameters of the ignition process caused by arc faults, the system employs multiple sensors to measure voltage, current, ignition time, smoke, temperature, and humidity. Arc voltage is recorded to determine arc duration, and together with current, is used to calculate the instantaneous power and cumulative energy of the arc fault. Flame sensors detect the precise moment when combustibles are ignited and fire is extinguished, while a smoke sensor array captures the distribution of smoke produced during combustion, assisting in the combustion state assessment of the combustibles. Temperature and humidity sensors are employed to record changes in the environment during experiments.

The data collection system utilizes the NI USB 6361 DAQ card for efficient data transmission to the supervisory computer, which then processes information visualization, manages data storage, performs detailed analyzes, and annotates datasets. Given the complexity and variability of arc fault experiments, this paper conducted repeated experiments to expand the data sample and quantify the results.

#### 4.2. Energy analysis of arc fault ignition

Fig. 9 shows the waveform data collected during the ignition experiment caused by arc faults. The signals gathered from various sensors collectively depict the complexity of the arc fault and its effects on the surrounding environment.

Initially, at  $t_{arc0}$ , the arc voltage swiftly increases from its baseline state, accompanied by significant distortion in the current waveform, highlighting the primary electrical characteristic of the arc fault. Subsequently, at  $t_{ignition}$ , the flame sensor signal dramatically intensifies, indicating the ignition of the cable's external combustible materials. Following this, at  $t_{smoke0}$ , the smoke sensor array starts detecting smoke, and the gradual increase in signals across different channels depicts the progression of the combustion process. Although the initial indicator of ignition is flame detection in specific wavelength bands, smoke detection also provides vital corroborative evidence that combustion has commenced. As shown in Fig. 10, the phase where arc faults and flame combustion coexist is typically marked by phenomena such as flame jets

and high-temperature particle splattering. Once the pre-determined arcing duration,  $t_{arc1}$ , is achieved, the arc voltage returns to the baseline, signaling the arc's extinction. At  $t_{extinguish}$ , the fallback of the flame sensor signal denotes the end of visible combustion, however, the combustibles can continue to burn with no visible combustion post arc fault. Following the extinguishing of the combustibles, the smoke density peaks and stabilizes at  $t_{smoke1}$  within a fully enclosed cover, reflecting the limited gas exchange in the experimental enclosure and the slow dispersion of smoke. The terms  $t_{arc0}$  to  $t_{arc1}$  denote the arc combustion duration,  $t_{ignition}$  to  $t_{extinguish}$  signify the duration of combustible material flame burning, and  $t_{smoke0}$  to  $t_{smoke1}$  indicates the time it takes for smoke to reach its peak from the initial detection.

Based on the described ignition process, it is observed that when an arc occurs, the high temperature causes the surrounding materials to undergo pyrolysis, decomposing and producing combustible gases. These gases are ignited when critical concentration is reached and sufficient heat is absorbed from sources, further heating the surrounding materials until conditions are met for sustained combustion. The energy required for ignition, defined as the ignition energy of an arc fault ( $Q_{ig}$ ), is a crucial parameter for assessing the ignition risk associated with arc faults. According to Eq. (2),  $Q_{ig}$  can be expressed as:

$$Q_{ig} = \int_{t_{arc0}}^{t_{ignition}} P_{arc}(t) dt = \int_{t_{arc0}}^{t_{ignition}} U_{arc}(t) I_{arc}(t) H(|I_{arc}(t)| - 0.05I_e) dt \quad (3)$$

$$\text{s.t. } H(x) = \begin{cases} 0 & \text{if } x \leq 0 \\ 1 & \text{if } x > 0 \end{cases}$$

The study in [20] indicates that the total energy released during the ignition process by arc faults is remarkably consistent across various  $I_e$ , maintaining a stable value of approximately 150 J. A similar but slightly higher energy range is reported in [21], further validating the consistency of energy release observed in previous studies. However, these findings contrast with the experimental results presented in this research. Data on the energy released by arc faults igniting external combustibles under varied  $I_e$  are systematically collected and analyzed. To differentiate between conditions that did or did not lead to the ignition of cotton, a support vector machine (SVM) model is employed to establish the decision boundary, with the upper and lower margins defining the optimal interval between two classes of sample data points. The distribution map in Fig. 11 shows the indistinct separation between the two classes, a phenomenon notably demonstrated by the overlap of sample data points. The results indicate that the arc fault energy required to ignite cotton shows a variability of 15 %–20 % under different current conditions, reflecting substantial instability. This variability, along with differences in the physical parameters of the experimental samples and types of combustible materials from those in previous studies, as well as the inherent randomness of the arc fault combustion process, contribute to understanding the instability in the relationship between ignition of combustible materials and energy

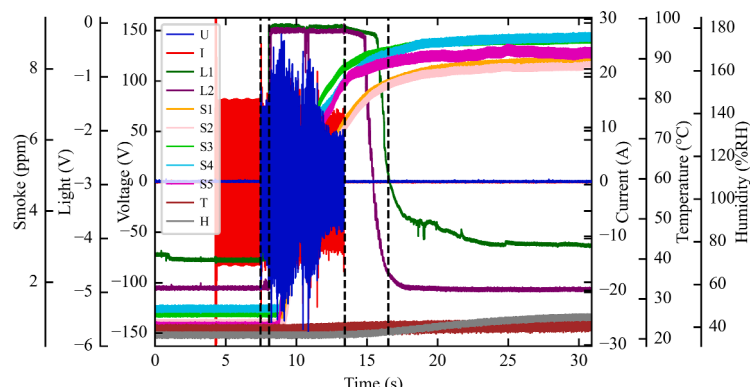


Fig. 9. Experimental waveforms of arc fault igniting external combustibles.

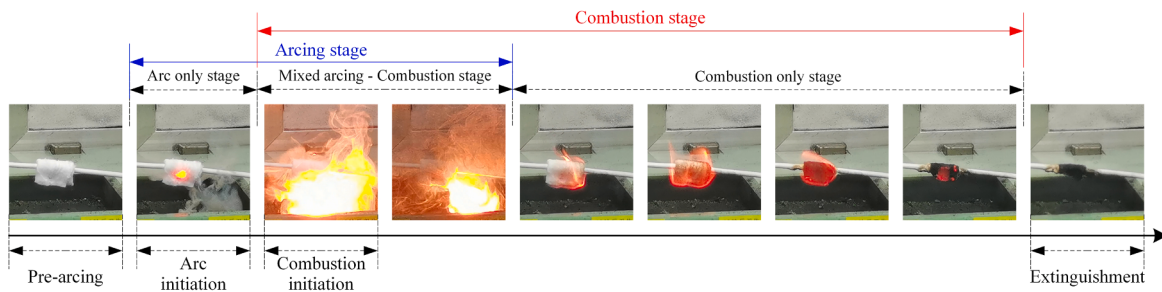


Fig. 10. Dynamic process of arc fault igniting external combustibles.

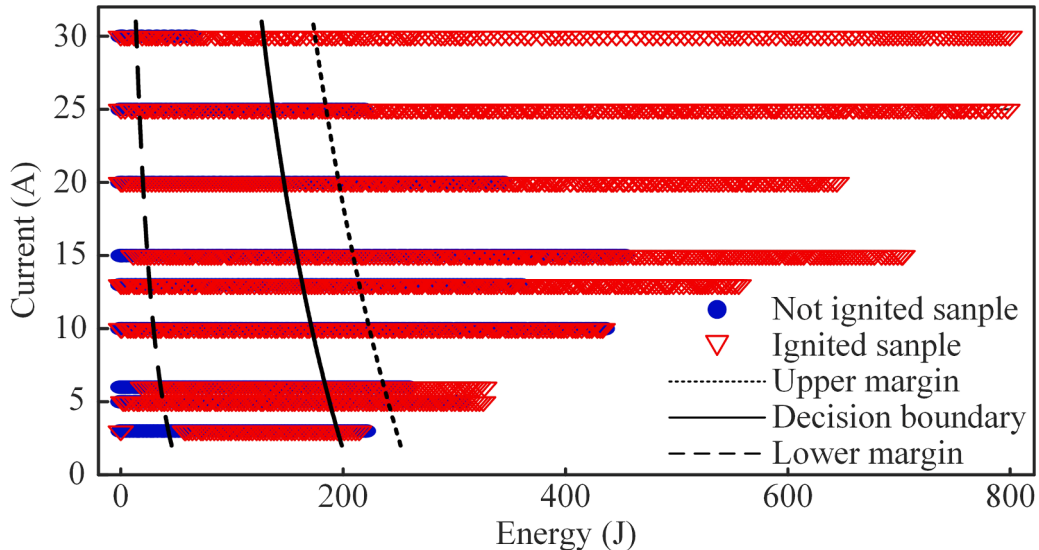


Fig. 11.  $I_e$  and  $Q_{ig}$  distribution under various fault conditions.

released by arc faults.

#### 4.3. Modeling arc fault ignition probabilities

A logistic regression (LR) model is employed to assess the impact of arc fault energy-related features on ignition probability. This model, suitable for simulating binary outcomes such as whether ignition occurs or not, is favored for its interpretability and efficiency. When considering multiple features, the LR model that describes ignition probability due to arc faults can be expressed as:

$$P(x) = \frac{1}{1 + \exp(-\beta_0 - \beta_1 x_1 - \beta_2 x_2 - \dots - \beta_n x_n)} \quad (4)$$

where  $x_1, x_2, \dots, x_n$  represent independent variables, and  $\beta_0, \beta_1, \dots, \beta_n$  are the model parameters. Parameter estimation within this model utilizes the MLE method, aiming to find parameters that maximize the probability of the observed sample data. The likelihood function  $L(\beta)$  represents the probabilities based on analysis of all observed data points, either ignition or no-ignition:

$$L(\beta) = \prod_{i=1}^n P(y_i|x_i; \beta)^{y_i} (1 - P(y_i|x_i; \beta))^{1-y_i} \quad (5)$$

where  $n$  is the number of samples,  $y_i$  and  $x_i$  represent the response and independent variables for the  $i$  th observation, respectively. The estimates of  $\beta$  are derived by maximizing  $L(\beta)$ . In practice, the maximization is simplified by taking the logarithm of  $L(\beta)$ , resulting in the log-likelihood function  $l(\beta)$  which can be expressed as:

$$l(\beta) = \sum_{i=1}^n [y_i \log(P(y_i|x_i; \beta)) + (1 - y_i) \log(1 - P(y_i|x_i; \beta))] \quad (6)$$

Gradient boosting is then applied to find the estimates of  $\beta$  that maximize the log-likelihood function. The ignition probability derived from the LR model not only provides an estimate of the likelihood of ignition events but also facilitates the analysis of how changes in independent variables affect ignition probability, thereby offering a robust tool for understanding and predicting ignition events.

After estimating the ignition probability using the LR model, the bootstrap method is employed to quantify the uncertainty of the prediction by calculating the confidence intervals (CI) for the model parameters. This method avoids presumptions about the parameter distribution, instead, it constructs an empirical distribution by repeatedly resampling and refitting the model with the original dataset. Parameters are estimated through the MLE method across numerous bootstrap iterations to obtain an empirical distribution, based on which the CI for each model parameter is calculated. For each parameter  $\beta_j$ , the 2.5 % and 97.5 % quantiles of the empirical distribution, denoted as  $\beta_{j,0.025}^*$  and  $\beta_{j,0.975}^*$ , are used to establish the CI. The 95 % CI for the parameter  $\beta_j$  is presented as:

$$CI_{0.95}(\beta_j) = [\beta_{j,0.025}^*, \beta_{j,0.975}^*]. \quad (7)$$

This interval provides a reliable measure for predicting ignition probability, reflects the inherent variability in predicting ignition probability, and offers a quantitative foundation for assessing ignition risk under various conditions.

#### 4.4. Ignition probability analysis under varied conditions

The random forest (RF) model is utilized to examine the correlation between the voltage, current, time-series features, and ignition labels, with  $I_e$  and  $Q_{ig}$  chosen as input parameters for the arc fault ignition probability model. Subsequently, LR model is employed to elucidate how these two parameters jointly affect ignition probability. Experiments at each  $I_e$  or load condition are repeated over 100 times to ensure the collection of stable and reliable data. Fig. 12 shows the frequency distribution of experimental samples of arc fault energy under certain current conditions. The histograms describe the sample number of observations for 'no ignition' (in blue) and 'ignition' (in red), with samples associated with ignition typically appearing in a higher energy range.

Given  $I_e$ , a series of  $Q_{ig}$  values are generated, and the ignition probability curve is plotted based on the fitted model. The bootstrap method is adopted to estimate the CI of the model prediction, thereby assessing the prediction's uncertainty. The number of resamples for Bootstrap is set at 1000, considering the computational costs and the time required. Fig. 13 shows the relationship between ignition probability and  $Q_{ig}$ - $I_e$  for Dataset 1 (resistive load case), with the shaded area depicting the 95 % CI.

The ignition probability curve displays the typical S-shaped distribution associated with the LR model under all  $I_e$  conditions. Notably, the curve lacks a saturation region at the minimum ignition probability, indicating the high sensitivity of arc fault ignition behavior to initial energy inputs. Even minimal levels of accumulated fault energy are sufficient to raise cable temperature under these conditions, subsequently increasing ignition probability. This finding underscores the importance of considering arc faults of lower energy levels since there are still ignition risks. The probability of ignition eventually approaches saturation as  $Q_{ig}$  increases, which demonstrates that  $Q_{ig}$  is a critical

factor for the likelihood of ignition events. A threshold exists in the saturation region, beyond which higher values of  $Q_{ig}$  have limited effects on increasing ignition probability, rendering ignition nearly certain. Moreover, Fig. 12 provides empirical support for the model as the observational data points for each  $I_e$  are distributed on either side of the curve.

The shapes of the ignition probability curve exhibit subtle differences under varying  $I_e$  conditions. High  $I_e$  values, such as 20A, generally correlate with a higher ignition probability compared to lower  $I_e$  values, such as 3A. Particularly at low  $I_e$ , the ignition probability increases with  $Q_{ig}$  at a slower rate, suggesting that the circuit may tolerate higher  $Q_{ig}$  levels for extended periods without ignition in the early stages of fault development. Conversely, at high  $I_e$ , the ignition probability curve shifts significantly to the left, reaching comparable ignition probabilities at lower  $Q_{ig}$  values. This behavior indicates that even brief exposures to high fault energy inputs are safety hazards. These trends reveal that  $I_e$  is another significant factor affecting ignition probability.

The CI of the model demonstrates higher predictive certainty indices for given values of  $I_e$  and  $Q_{ig}$ . Variations in the CI across different  $I_e$  values reflect performance stability and predictive certainty under diverse data conditions. Specifically, a narrower CI at lower  $I_e$  levels suggests increased predictive confidence. Meanwhile, overlapping CI saturation curves at higher energy levels show diminishing differences between currents. This pattern is attributed to the randomness in the intensity of arc fault combustion across various  $I_e$  levels.

Fig. 14-(a) and (b) show the ignition probabilities for Datasets 2 and 3, respectively. Dataset 2 involves an inhibition load (inhibition test A in the IEC/GBT standard: 4.38A-9.2A), while Dataset 3 includes an inhibition load in parallel with a 3A resistor (inhibition test D in the IEC/GBT standard: 4.11A-12.2A). Irrespective of the load conditions, the ignition probability curves follow the previously described trends. There

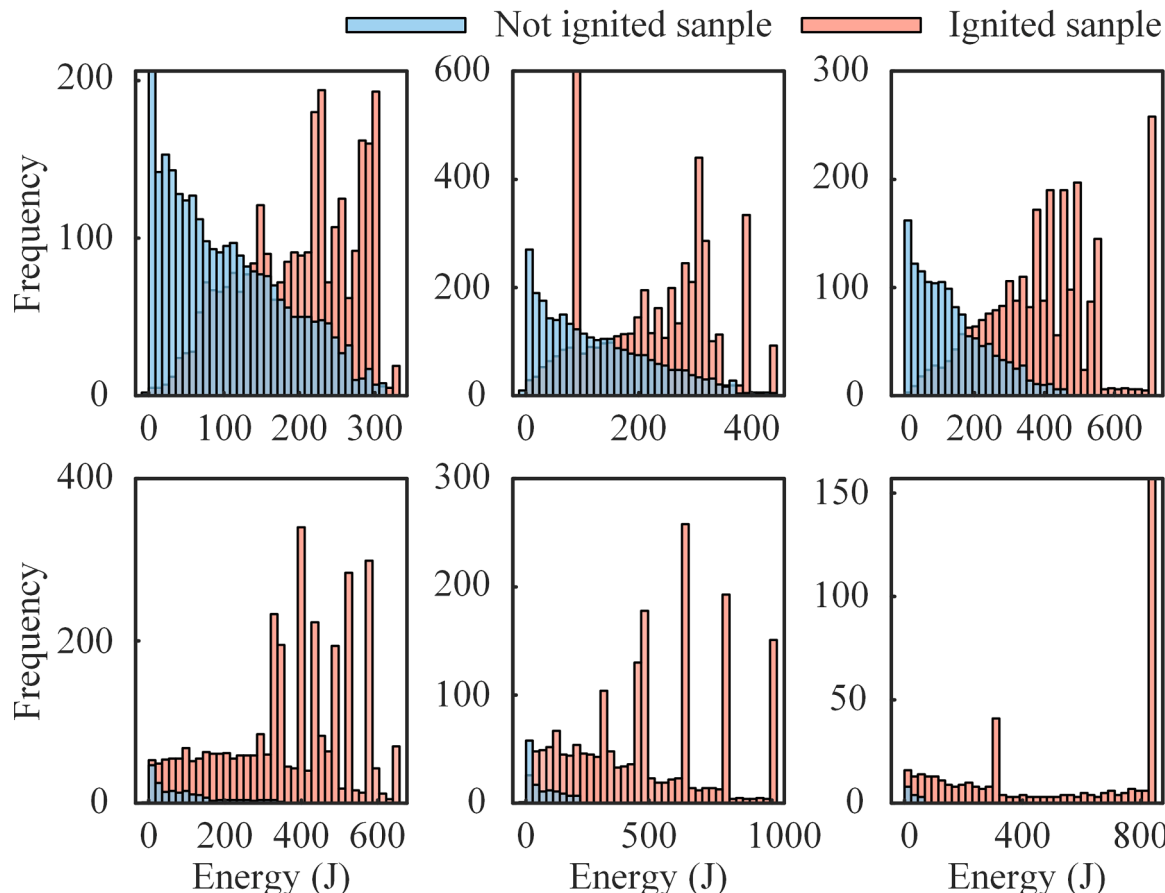
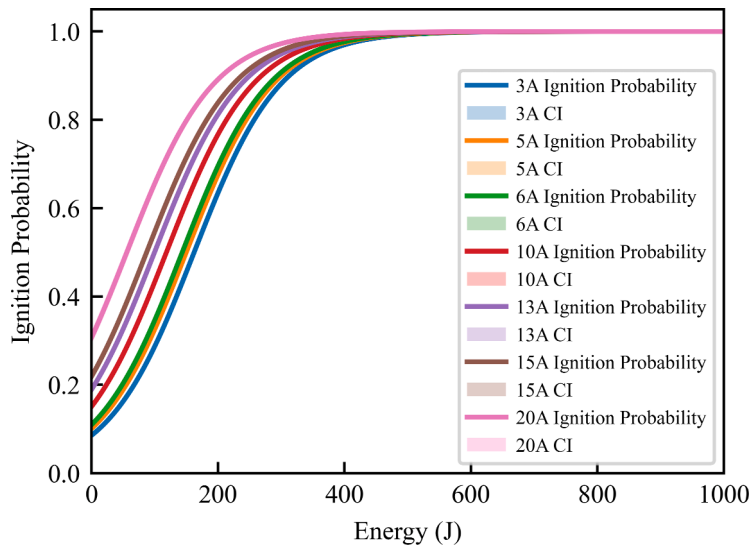
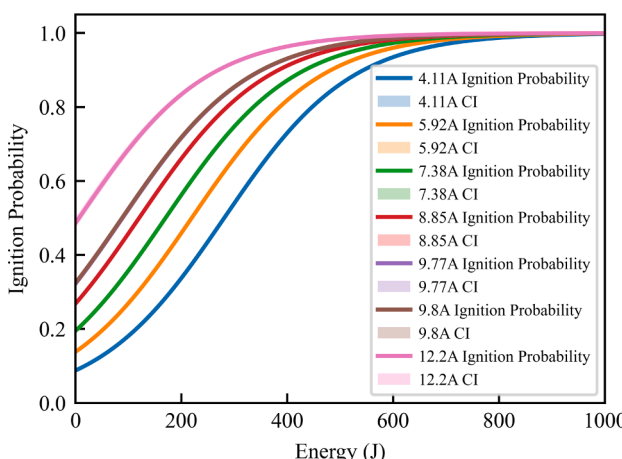
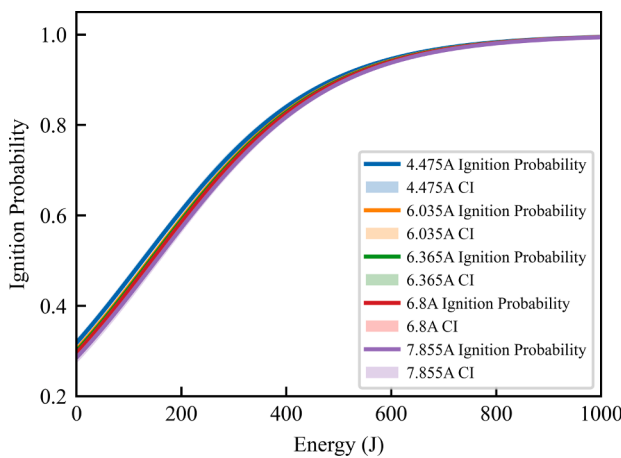


Fig. 12. Sample frequency distribution under certain current conditions.



**Fig. 13.** Ignition probability curves under resistive loads.



**Fig. 14.** Ignition probability curves under inhibition loads. (a) Inhibition test A, (b) Inhibition test D.

exists a  $Q_{ig}$  threshold that is independent of the load type and circuit configuration; once this threshold is exceeded, the probability of ignition swiftly approaches certainty. The impact of  $I_e$  on ignition probability aligns with that shown in Fig. 13, where higher  $I_e$  correlates with

increased ignition likelihood. Under inhibition loads, despite the reduced range and intervals of  $I_e$ , the fundamental shape of the ignition probability curves across different  $I_e$  levels remains consistent, and the CI of the curve under inhibition load conditions continues to reflect the predictive certainty of the probability model.

The inclusion of inhibition loads and their parallel resistors can alter the characteristics of arc faults and ignition probabilities, leading to nuanced differences in the shape of the ignition probability curves. The slopes and contours of these curves under various conditions differ, indicating how the complexity of the load settings affects the ignition process. Under the condition of a single inhibition load, the initial ignition probability is higher, yet the curve's slope remains relatively stable compared to resistive conditions, necessitating higher energy levels to reach the saturation area. The addition of a parallel resistor modifies the arc fault characteristics of the inhibition load, causing its curve shape to more closely resemble that of resistive conditions.

#### 4.5. Comparative performance of different probability methods

The effectiveness of the proposed method is compared with those derived from three models: SVM, RF, and Gradient Boosting (GB), in predicting arc fault ignition probability. Utilizing a consistent experimental framework, all methods employ the same parameters and Bootstrap resampling settings as outlined in Section IV.D. Each method is trained and tested on identical datasets. The training dataset includes all data from Datasets 1–3, while the test dataset, fixed at a 5A current level, spans the minimum to the maximum range of  $Q_{ig}$ .

The predictive performance of all methods is evaluated through the relationship curve between ignition probability and energy, as shown in Fig. 15-(a). The overall trends in ignition probability predictions across various energy levels remain consistent among methods. The MLE method displays a smooth curve for ignition probability. The RF and GB methods exhibit significant fluctuations at lower energy levels, whereas the SVM method does the opposite.

The energy range is segmented into low, medium, and high levels to investigate the performance of various methods in predicting ignition probability. The predictive accuracy and uncertainty of each method are assessed using the CI range, which indicates the predictive certainty expressed by the CI, across the energy levels. Fig. 15-(b) demonstrates that the MLE method consistently exhibits lower uncertainty across all energy levels, especially in the low and high energy segments, where the correspondent CI is remarkably more consistent compared to other methods. This robustness underscores the MLE method's capability to

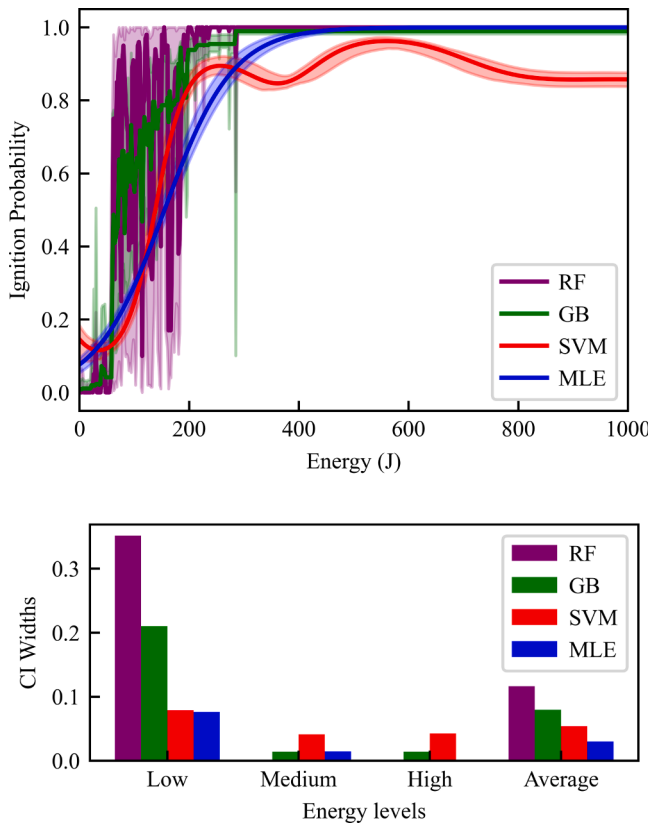


**Fig. 15.** Comparison of ignition probability prediction by different methods. (a) Ignition probability curve, (b) CI Widths across all energy levels.

minimize variability under diverse extreme conditions. In contrast, the RF and GB methods display a wider range of CIs in the low energy segment, indicating prediction instability of tree-based models when dealing with significant data fluctuations. Nonetheless, these methods achieve moderate prediction stability across most cases of the high energy segment. The SVM method performs optimally in the medium energy segment but shows increased uncertainty at extreme energy values. Additionally, the MLE-based method maintains a narrower range of average CI widths across the entire energy spectrum than the other methods, further confirming its consistent accuracy and stability at various energy levels.

In summary, the proposed method excels with superior accuracy and stability. However, selecting the most suitable method depends on the specific requirements of applicative scenarios, including data complexity, predictive stability, and resource availability. For instance, the SVM-based method demonstrates resilience to data volume variations and maintains consistent ranges of CI indices across energy levels, making it particularly appropriate for cases involving high-dimensional data.

## 5. Experimental analysis

AFDDs are engineered to mitigate the hazards associated with arc faults. The ignition probabilities at various current levels, within the mandatory time constraints of relevant standards, are evaluated by comparing the required action times for AFDDs under the GB/T 31143 and IEC 62606 standards. Subsequently, through performance evaluations of seven AFDD prototypes under diverse experimental conditions, the efficacy of AFDDs in reducing fire risks caused by arc faults is further investigated.

### 5.1. Ignition probability within AFDD standards

The GB/T 31143 and IEC 62606 standards delineate maximum break times for AFDD actions at various current levels, with notable differences between the two. These variations significantly influence the potential for arc fault ignition and, consequently, the effectiveness of AFDD technology in fire prevention. The former sets a maximum break time for AFDD action for currents of 20A and below, as shown in Table 1. In contrast, the latter enforces shorter break times for AFDDs to complete actions at the same current levels, reflecting a more stringent requirement for arc fault protection. When the current applied to the circuit is not one of the specified values, the allowable break time shall be determined by linear interpolation between the break time values above and below the actual current.

Experiments are conducted 50 times across various current levels to determine the average arc fault energy per period. Using the ignition probability model, the average ignition probabilities at the break time limits of the GB/T standard are calculated, as shown in Table 1. Despite circuit interruption within these break time limits, the probability of external combustibles ignited by arc faults remains, and the probability increases with higher current levels.

A comparative analysis of the ignition probabilities under the maximum break times of the GB/T and IEC standards reveals significant differences. The IEC 62606 standard, characterized by stricter break time limits across different current levels, exhibits superior performance in reducing ignition risks. Specifically, for currents below 20A, the IEC standard achieves an average reduction in ignition probability of 12.1 %, as shown in Fig. 16. This substantial difference underscores the enhanced safety provided by the IEC standard in the range of lower current magnitudes, critical for household and light-load commercial applications. However, at higher current levels above 40A, both standards exhibit minimal differences in mandatory break times and offer similar protection against arc faults in scenarios typically associated with industrial or heavy-duty commercial applications.

These findings have significant implications for the implementation and enhancement of AFDD technology: (a) Enhanced low-current protection: Given the superior performance of the IEC 62606 standard at low current magnitudes, it is advisable to tighten the GB/T 31143 requirements further. Local standards, particularly those for residential and light-load commercial settings where lower current magnitudes are prevalent, should be made more stringent to provide better protection. (b) Uniform high-current performance: The similar requirement of both standards at high currents levels suggests that AFDDs compliant with either standard can provide adequate protection in industrial environments. (c) Room for improvement: While both standards contribute to reducing ignition risks, neither completely eliminates the possibility of ignition. Given the fixed operating times of circuit breakers, it is essential to enhance the speed and accuracy of arc fault detection technology to improve the responsiveness and overall safety of AFDD systems. (d) Regulatory considerations: Policymakers and safety regulators should consider these differences when adopting or updating standards, potentially favoring the more stringent IEC 62606 standard for comprehensive arc fault protection.

Overall, although the action time constraints imposed by both standards help mitigate the ignition of external combustibles caused by arc faults, the IEC 62606 standard shows higher effectiveness, especially

**Table 1**  
Limit values of break time under GB/T 31143.

Current (A)	Break time (s)	Average arc fault energy (J)	Average ignition probability
3	1	2.33	33.92 %
6	0.5	3.82	33.16 %
13	0.25	6.87	44.98 %
20	0.15	9.15	54.65 %

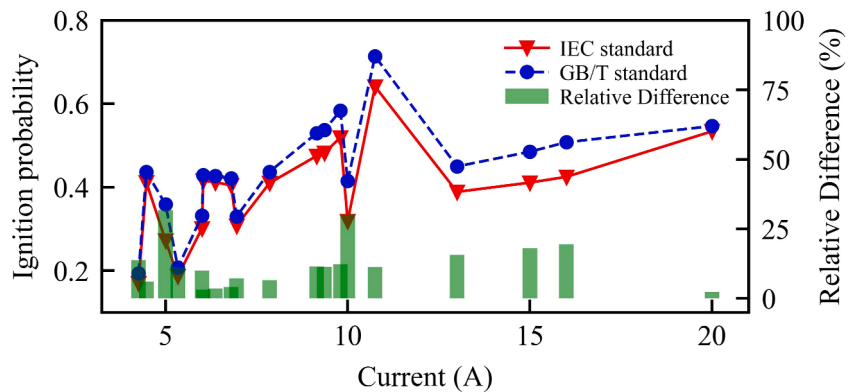


Fig. 16. Ignition probability at different current levels according to GB/T and IEC standards.

in low-current scenarios. However, the continued presence of ignition risks, even within standard-compliant break times, underscores the necessity for ongoing advancements in AFDD technology and potentially stricter safety standards.

### 5.2. Ignition probability with AFDD prototypes

AFDDs are engineered to detect and interrupt arc faults, thereby safeguarding circuits from related hazards. The maximum break time set by standards is directed against the worst-case scenario, where an arc fault persists at a specific current level. However, in practical scenarios, AFDDs frequently aim to complete the interruption action more swiftly and accurately. Therefore, this paper adopts a quantitative approach to assess the performance of AFDDs, focusing on the arc fault energy before interruption to evaluate the effectiveness of devices in mitigating fire risks associated with arc faults.

To ensure the reliability of the results, seven AFDD prototypes are selected, and three tests aligned with standard requirements are carried out in the experimental setup. The experimental project includes standard tests for sudden appearance of series arc in the circuit, inserting a load with series arc fault, closing on series arc fault, and masking test with inhibition loads (topology A and D)/EMI filter/line impedance. These experiments encompass a comprehensive analysis of series arc faults. The experimental results are detailed in Table 2, where Tot. denotes the total number of experimental projects selected; P. represents the projects that complied with the standard's time constraints; FT. denotes prototypes that interrupted the fault but not within the prescribed time; FNT. signifies prototypes that failed to interrupt; Pi-P., Pi-F., and Pi-Tot. indicate the ignition probabilities of the prototypes in passing, failing, and across all projects, respectively.

The data presented in Table 2 shows variations in performance across different AFDD prototypes during arc fault experiments. In addition to disparities in break times and energies, the pass rate distinctly mirrors the capability of each prototype to successfully interrupt and break the circuit within the designated time. The pass rates among the prototypes range from 100 % for Prototype 2 to 42.31 % for Prototype 7.

The Pi-P. is typically around 30 %. Although this result represents a

significant improvement over the nearly 100 % ignition probability without AFDD intervention, there is still a fire risk when AFDDs function properly. Notably, Prototypes 5 and 7 exhibit lower Pi-P. values due to their rapid response only in low current fault experiments.

The Pi-F. is generally above 70 %, underscoring the substantial increase in fire risk when AFDDs fail to interrupt the circuit within the designated time. For these projects, Prototype 4 showed an exceptionally high Pi-F. due to inadequate detection and response capabilities under high current fault conditions. In contrast, the reason the Pi-F. of Prototype 3 is below 70 % is that it fails to act normally only under low current conditions that combine a filter with a 3A resistance, attributable to the configuration of the EMI filter.

The Pi-Tot. of the prototypes and its inverse relationship with the pass rate offer additional insights into the correlation between AFDD circuit-breaking performance and fire risk. As indicated by the ignition probability curve in Section IV.D, the prompt completion of actions conducted by AFDDs can significantly mitigate fire risks associated with arc faults. An exception is Prototype 7, which, despite a lower pass rate, has a Pi-Tot. comparable to Prototype 6. This is attributed to the lower rated current of Prototype 7, with its failures predominantly occurring at medium and low current levels, and relatively smaller FNT.

In summary, the results emphasize the vital role of AFDDs in mitigating the risk of electrical fires caused by arc faults. While the mandatory break times of standards represent the basic safety requirements in most severe experimental scenarios, AFDDs generally detect arc faults and disconnect circuits more swiftly, thus substantially lowering the fire risk.

## 6. Conclusion

The widespread occurrence and correspondent safety hazard of arc faults in residential environments underscore the importance of understanding the dynamic characteristics and ignition capabilities of arc faults to improve the safety and operational integrity of power systems. The detailed voltage/current data and ignition-related information are collected through an arc fault experimental system and an integrated multi-sensor data collection system. Further analysis reveals a significant correlation between arc fault energy and ignition probability across various current levels.

An MLE method for ignition probability, based on  $I_e$  and  $Q_{ig}$ , proves effective and accurate in predicting ignition events resulting from arc faults. The 95 % CI of the model is determined using the Bootstrap method, thereby confirming its stability and reliability under diverse data conditions. A comparison of the GB/T 31143 and IEC 62606 standards using the proposed model shows that the latter reduces the average ignition probability by 12.1 % under stricter time constraints. Notably, experiments with seven AFDD prototypes demonstrated that when AFDDs operate within the maximum break time limits of the standards, the ignition probability significantly decreases to below 30

Table 2  
The experimental data of AFDD prototypes.

Prototype	Tot./P.	FT./FNT.	Pass rate	Pi-P.	Pi-F.	Pi-Tot.
1	27/23	3/1	85.19 %	33.46 %	73.18 %	39.34 %
2	26/26	0/0	100.00 %	29.39 %	none	29.39 %
3	28/26	2/0	92.86 %	30.05 %	61.77 %	32.32 %
4	30/27	3/0	90.00 %	34.15 %	87.21 %	37.29 %
5	29/21	7/1	72.41 %	26.84 %	73.50 %	39.71 %
6	27/14	1/12	51.85 %	31.07 %	77.31 %	53.33 %
7	26/11	5/10	42.31 %	25.96 %	73.11 %	53.16 %

%, highlighting the efficacy of AFDD technology in mitigating fire risks associated with arc faults. However, for AFDDs that do not meet the standards, the ignition probability ranges between 30 % and 60 %, emphasizing the importance of AFDD standards.

The arc fault ignition probability model introduced in this paper establishes a scientific foundation and offers data support for enhancing arc fault detection and fire prevention strategies. By evaluating the consistency of AFDD actions and the variability of ignition mechanisms observed in experiments, the model validates its applicability in the design and experimental guidance of AFDDs, simultaneously fostering the selection of optimal balance between sensitivity and ignition probability. This method is anticipated to integrate further into dynamic monitoring and early warning systems, assessing arc fault risks in real-time and providing a crucial window for implementing preventive actions. Moreover, this approach can expand to include arc fault traceability and fire cause analysis, increasing the precision of fire causation assessments based on-site arc fault data and model predictions. Future studies may incorporate more data concerning historical buildings and museums destroyed and lost due to arc fault fires while dedicating to developing more comprehensive experimental systems tailored to various building circuits and specific settings. The continued improvement in understanding arc fault characteristics and related ignition phenomena across diverse applicative scenarios has the potential to remarkably enhance electrical safety, especially for residential environments. Ultimately, this work will offer a more accurate scientific basis for fire investigations and the development of related safety standards.

#### CRediT authorship contribution statement

**Liwei Du:** Writing – original draft, Software, Methodology, Investigation, Conceptualization. **Yulong Shen:** Writing – review & editing, Validation, Formal analysis. **Zhihong Xu:** Project administration, Funding acquisition, Formal analysis. **Lijun Chen:** Data curation. **Duanyu Chen:** Resources, Formal analysis.

#### Declaration of competing interest

The authors declare that they have no known competing financial interests or personal relationships that could have appeared to influence the work reported in this paper.

#### Acknowledgments

This work is supported by National Natural Science Foundation of China (52277136) and Science and Technology Project of State Grid Fujian Electric Power (52131024000F).

#### Data availability

Data will be made available on request.

#### References

- [1] Y. Wang, L. Hou, K.C. Paul, Y. Ban, C. Chen, T. Zhao, ArcNet: series AC arc fault detection based on raw current and convolutional neural network, *IEEE Trans. Industr. Inform.* 18 (1) (Jan. 2022) 77–86.
- [2] Y. Zhang, et al., Lightweight AC arc fault detection method by integration of event-based load classification, *IEEE Trans. Ind. Electron.* 71 (4) (Apr. 2024) 4130–4140.
- [3] X. Tang, Z. Zhang, J. Ren, Q. Huang, W.J. Lee, Resilience enhancement aimed adaptive identification of arc fault in distribution system, *IEEE Trans. Ind. Appl.* 60 (2) (Mar-Apr. 2024) 2312–2320.
- [4] A. Chabert, P. Schweitzer, S. Weber, J. Andrea, State-space simulation of electric arc faults, *IEEE Trans. Aerosp. Electron. Syst.* 58 (3) (Jun. 2022) 1650–1659.
- [5] L. Du, Z. Xu, H. Chen, D. Chen, Feature selection-based low-voltage ac arc fault diagnosis Method, *IEEE Trans. Instrum. Meas.* 72 (Oct. 2023) 1–12.
- [6] L. Du, Y. Shen, Z. Xu, D. Chen, Enhancing arc fault diagnosis method using feature selection strategy based on feature clustering and maximal information coefficient, *IEEE Trans. Ind. Appl.* 60 (2) (Mar-Apr. 2024) 3006–3017.
- [7] J. Gao, M. Guo, S. Lin, D. Chen, Application of semantic segmentation in high-impedance fault diagnosis combined signal envelope and hilbert marginal spectrum for resonant distribution networks, *Expert Syst. Appl.* 231 (2023) 120631.
- [8] K. Takenaka, Y. Ishikawa, Y. Mizuno, W. Lin, Arc discharge - induced ignition of combustibles placed on a damaged AC power supply cord, *Energies. (Basel)* 13 (3) (Feb. 2020) 681.
- [9] D. Kolker, S. Campolo and N. DiSalvo, “A study of time/current characteristics of the ignition processes in cellulosic material caused by electrical arcing for application in 240V arc-fault circuit interrupters,” *Electrical Contacts - 2007 Proceedings of the 53rd IEEE Holm Conference on Electrical Contacts*, Pittsburgh, PA, USA, 2007, pp. 105–114.
- [10] J.K. Hastings, M.A. Juds, C.J. Luebke and B. Pahl, “A study of ignition time for materials exposed to DC arcing in PV systems,” *2011 37th IEEE Photovoltaic Specialists Conference*, Seattle, WA, USA, 2011, pp. 3724–3729.
- [11] J. Yang, R. Zhang, L. Huang, Study on measuring method and experiment of arc fault detection device, *Appl. Mech. Mater.* 870 (Sept. 2017) 342–347.
- [12] F. Ge, T. Qiu, M. Zhang, J. Ji, Experimental research on the thermal characteristic of low-voltage alternating current (AC) arc faults, *Fire Saf. J.* 136 (Apr. 2023) 103732.
- [13] J.J. Shea, Identifying causes for certain types of electrically initiated fires in residential circuits, *Fire Mater.* 35 (1) (Jan. 2011) 9–42.
- [14] M. Zheng, X. Wu and G. Yan, “Investigation on fault arc energy under different load based on the new time varying resistance fault arc model,” [in Chinese], *Electric Power*, vol. 48, no. 11, pp. 49–53, Nov. 2015.
- [15] R. Grassetti, R. Ottoboni, M. Rossi, S. Toscani, Low cost arc fault detection in aerospace applications, *IEEE Instrum. Meas. Mag.* 16 (5) (Oct. 2013) 37–42.
- [16] K.M. Armijo, J. Johnson, R.K. Harrison, K.E. Thomas, M. Hibbs, A. Fresquez, Quantifying photovoltaic fire danger reduction with arc-fault circuit interrupters, *Prog. Photovolt.: Res. Appl.* 24 (4) (Apr. 2016) 507–516.
- [17] N. El-Sherif, T.A. Domitrovich, Demystification of arc-fault circuit-interrupters: part I: beginning of the odyssey, *IEEE Ind. Appl. Mag.* 30 (3) (May-Jun. 2024) 18–27.
- [18] J. Martel, M. Anheuser and F. Berger, “Time-current tripping characteristics at series arcing for arc fault detection devices,” *ICEC 2014; The 27th International Conference on Electrical Contacts*, Dresden, Germany, 2014, pp. 1–6.
- [19] J.M. Martel, M. Anheuser and F. Berger, “A study of arcing fault in the low-voltage electrical installation,” *2010 Proceedings of the 56th IEEE Holm Conference on Electrical Contacts*, Charleston, SC, USA, 2010, pp. 1–11.
- [20] W.S. Moon, J.C. Kim, A. Jo, S.B. Bang, W.S. Koh, Ignition characteristics of residential series arc faults in 220-V HIV wires, *IEEE Trans. Ind. Appl.* 51 (3) (May-Jun. 2015) 2054–2059.
- [21] W.S. Ko, W.S. Moon, S.B. Bang, J.C. Kim, Analysis of ignition time/current characteristics and energy when series arc-fault occurs at rated 220 V, *The Trans. Korean Inst. Electr. Eng.* 62 (8) (Aug. 2013) 1184–1191.
- [22] N. Kang, Zhao Z, J. Lin, S. Lu, Ignition of silicone rubber sheaths by series arcs at different currents and durations, *Fire Saf. J.* 136 (Apr. 2023) 103753.
- [23] C. Vasile, V. D'Orchymont, J. Meunier-Carns, J.F. Rey and H. Raisigel, “Arcing persistency measurement for IEC62606 arc-fault detection device certification,” *2019 IEEE Symposium on Product Compliance Engineering (SPCE Austin)*, Austin, TX, USA, 2019, pp. 1–6.
- [24] General Requirements for Arc Fault Detection Devices (Edition 1.1), Geneva, Switzerland, 2017.
- [25] General Requirements for Arc Fault Detection Devices (AFDD), Beijing, China, 2014.
- [26] Electrical Fire Monitoring System - Part 4: Arcing fault Detectors, Beijing, China, 2014.
- [27] UL Standard for Arc-Fault Circuit-Interrupters (Third Edition), New York, NY, USA, 2017.
- [28] L. Du, Z. Xu, D. Chen, Improved control strategy for carbonized cable preparation in low-voltage arc fault test, *Chin. J. Electr. Eng.* 9 (4) (Dec. 2023) 122–131.
- [29] J. Du, R. Tu, Y. Zeng, L. Pan, R. Zhang, An experimental study on the thermal characteristics and heating effect of arc-fault from Cu core in residential electrical wiring fires, *PLoS. One* 12 (8) (Aug. 2017).
- [30] E. Carvou, J.L. Le Garrec, J.B.A. Mitchell, Characteristics of arcs between porous carbon electrodes, *IEEE Trans. Plasma Sci.* 41 (11) (Nov. 2013) 3151–3158.
- [31] W. Wu and Z. Xu, “Design of arc generator based on electromechanical coupling closed-loop fuzzy control,” *Proceedings of 2021 Chinese Intelligent Systems Conference*, Singapore, 2022, pp. 547–560.
- [32] M. Zhang, F. Ge, H. Hu, J. Ji, Experimental research on the fault arc arcing process and electrode temperature distribution of a 220VAC power system, *Int. J. Therm. Sci.* 199 (May. 2024) 108895.
- [33] J.C. Kim, D.O. Neacșu, R. Ball, B. Lehman, Clearing series ac arc faults and avoiding false alarms using only voltage waveforms, *IEEE Trans. Power Deliv.* 35 (2) (Apr. 2020) 946–956.